

Effect of Impact Angle on Slurry Erosion Behaviour and Mechanisms of Carburized AISI 5117 Steel

Y. M. Abd-Elrhman¹, A. Abouel-Kasem², K.M. Emar³, S. M. Ahmed⁴

1-Mechanical Engineering Department, Faculty of Engineering, Assiut University, Assiut71516, Egypt

E-mail: y_mahmoud_a@hotmail.com

2-Mechanical Engineering Department, Faculty of Engineering, King Abdulaziz University, 344 Rabigh 21911, Kingdom of Saudi Arabia,

Also, Mechanical Engineering Department, Faculty of Engineering, Assiut University, Assiut71516, Egypt

E-mail: abouelkasem@yahoo.com

3-Mechanical Engineering Department, Faculty of Engineering, Assiut University, Assiut71516, Egypt

E-mail: emara@aun.edu.eg

4-Mechanical Engineering Department, Faculty of Engineering, Majmaah University, North Riyadh, Kingdom of Saudi Arabia

E-mail: shemy2007@yahoo.com

(Received September 11, 2012 Accepted October 8, 2012)

Abstract

The paper reports a study of slurry erosion of carburized AISI 5117 steel using whirling-arm rig. The study is mainly focused on studying the erosion wear resistance properties of AISI 5117 steel after carburizing at different impact angles. The mechanisms of erosion wear at different impact angles are presented using SEM examination of eroded samples. In addition, the SEM images of eroded samples at different stages are presented for better understanding of erosion mechanisms at different angles. The tests were carried out with particle concentration of 1 wt %, and the impact velocity of slurry stream was 15 m/s. Silica sand having a nominal size range of 250 – 355 μm was used as an erodent. The results showed that, carburizing process of steel increased the erosion resistance and hardness compared with untreated material for all impact angles. The erosion resistance of AISI 5117 steel increases by 70, 57, 60 and 36 % at an impact angle of 30°, 45°, 60° and 90°, respectively as result of carburizing, i.e. the effectiveness of carburizing was the highest at low impact angles. Treated and untreated specimens behave as ductile material, and the maximum mass loss appears at impact angle of 45°. Plough grooves and cutting lips appears for acute impact angle, but the material extrusions are for normal impact angles. The erosion traces are wider and deeper for untreated specimens comparing by the shallower and superficial ones for the carburized specimens.

Keywords: Slurry erosion; carburizing; impact angle; AISI 5117 steel; wear resistance; erosion mechanisms.

1. Introduction

In mining, marine, chemical, oil gas, power generation industries and power transmission and building material industries, components of equipment which transport various slurries often fail in a relatively short time. This problem has been, and still of important world-wide concern and many researchers have been done on this topic [1–6]. Usually, steels used in slurry equipment are subjected to some processes of surface treatment to improve their erosion resistance. One of these processes is carburizing. Carburizing is the addition of carbon to the surface of low-carbon steels at temperatures (generally between 850 and 950 °C) at which austenite, with its high solubility for carbon, is the stable crystal structure. Hardening is accomplished when the high-carbon surface layer is quenched to form martensite so that a high-carbon martensitic case with good wear and fatigue resistance is superimposed on a tough, low-carbon steel core. Of the various diffusion methods pack carburizing is one of the most widely used surface hardening processes. This method has the following advantages: ease of operation; adaptability and portability of its equipment; ability to heat-treat component after surface-finishing (since there is little oxidation, decarburization or distortion); and the ease of producing deeper zones of case depth. AISI 5117 steel, which is an alloy steel, is used for machine elements such as cam shafts, gears and other power transmission elements after surface being treated by carburizing or nitriding. It has been shown that [7-9], carburizing has improved the tribological properties of low carbon steel. Despite the fact that, the relationship between the increasing hardness of steels and enhanced erosion performance is well recognized in field practice, attempts to simulate such wear conditions in the laboratory and to provide the required data have not been marked by significant success.

The impact angle is one of the major test parameters that is associated with turbine operating conditions. Hydro turbine components are subjected to a wide range of impact angles at different locations [10]. Hence, an investigation of the erosion rate at different impact angles for carburized and untreated specimens gives an idea of the maximum erosion rate that may occur in particular test conditions.

The aim of this study is to characterize the slurry erosion behaviour of carburized alloy steel AISI 5117 with the change of impact angle.

2. Experimental details

2.1 Materials

The test specimens were made from a commercial grade of alloy steel, namely AISI 5117. This type of Alloy steel is used because it provides good machinability and behaves well during heat treatment and quenching with respect to distortion, internal stresses and mechanical properties of surface and core. The chemical composition and mechanical properties of the specimen material are listed in Tables 1 and 2, respectively.

Table 1 Chemical composition of low alloy steel AISI 5117 [11]

Element	C	Si	Cr	Mn	S	P	Fe
Wt. %	0.17	0.3	0.9	1.2	0.003	0.005	Balance

Table 2 Mechanical properties of low alloy steel AISI 5117 [11]

Yield Strength(MPa)	Tensile Strength (MPa)	Modulus of Elasticity (GPa)	Hardness, Hv (200g)	Density (kg/m ³)
600	950	210	200	7850

The test samples were machined from the above material in the shape of rectangular blocks with dimensions 23 mm × 10 mm × 10 mm. Prior to carburizing process, surface of specimens were polished using silicon carbide abrasive paper and cleaned by acetone to remove oxide layers and irregularities in order to enhance carbon uniformity. The specimens were packed in a stainless steel box filled with charcoal powder (carburizing agent) with 10% of calcium carbonate to prevent caking. The box was first filled with the carburizer compound about 20 mm thick which was then rammed flat and the specimens were placed about 25 mm away from the sides of the carburizing box. The specimens were carburized at a temperature of 950°C for two different carburizing times of 6 and 12 h. All the specimens were quenched from the carburizing temperature in salt water and then they were tempered at 200°C for one hour. Some of the treated specimens were sectioned, polished and etched with 2% nital solution for microstructure examination. Vickers microhardness was conducted using a Highwood HWDM-3 (TTS Unlimited Inc., Japan) instrument at load of 200 g. The microhardness profile was done using sample cross-sections. While the erosion specimens were carefully polished with silicon carbide abrasive papers up to 4000 grit. The weight losses were determined by using an analytic balance having sensitivity of 0.1 mg. Erosion specimens were cleaned by acetone and dried by an air blower before and after the test.

2.2 Slurry erosion testing procedure

Slurry erosion tests were performed using a slurry whirling arm rig, which is shown schematically in Figure 1. The rig consists of three main units: a specimen rotation unit, a slurry unit, and a vacuum unit. Full description of this rig and how it works as well as its dynamics are found in Ref. [12-15]. Two specimen holders are mounted on the ends of two aligned arms, which are tightened firmly to the whirling rotator and balanced for high-speed operation. The effective rotation diameter of the whirling arms is 248 mm. The rotor is driven by a variable speed motor. The specimen holders have tilting and locking facilities to adjust the required inclination of the test specimen. The specimen rotation unit provides impact velocity. During slurry erosion tests, only the front surface of specimen is exposed to the impinging slurry since the sides of the specimen are held by the specimen holder. The front surfaces of the specimens, test surfaces, were of dimensions 23 mm × 10 mm. The impact angle can be adjusted to a required value by rotating the specimen holder around its horizontal axis as shown in Figure 2. The holders are mounted on the ends of the two arms of the rotator which is driven by a variable speed motor.

The used slurry whirling arm rig provides a homogenous stable slurry stream (a mixture of tap water and SiO₂). The velocity of falling slurry stream from the 3 mm diameter funnel orifice is 1.67 m/s, at the specimen surface, impacting every specimen at any pre-set angle between 0 deg and 90 deg. The impact angle (θ) and impact velocity (v) are correlated to ensure the intended value, which can be obtained from the velocity vector diagram of particle impact, as shown in Figure 2. The distance between the funnel orifice and the specimen surface is 40 mm. The slurry test chamber is evacuated by a vacuum system (up to 28 cm Hg) to eliminate aerodynamic effects on slurry system.

Natural silica sand, sieved to a nominal size range of 250 – 355 μm was used as an erodent. A scanning electron microscope (SEM) photograph of typical sand particles is shown in Figure 3. These particles were characterized using an image analysis method in terms of the aspect ratio (W/L) and roundness factor ($P^2/4\pi A$), where W is the particle width, L is the particle length, A is the projected area of the particle, and P is its perimeter. The statistical values of the particle parameters are given in Table 3.

Table 3 Statistical values of particle size and shape as obtained by image analysis of SiO₂ particles

Particle size range(μm)	Statistical parameters	Area $A(\mu\text{m}^2)$	Average diameter $D(\mu\text{m})$	Length, $L(\mu\text{m})$	Width, $W(\mu\text{m})$	Aspect Ratio, W/L	Perimeter, $P(\mu\text{m})$	$P^2/(4\pi A)$
250-355	Mean	76336.88	301.10	387.08	272.76	0.7180	1117.48	1.36
	Median	76040.1	300.99	375.81	276.32	0.736	1108.79	1.25
	Standard deviation	20,507.5	43.60	64.29	44.68	0.14	161.34	0.38

Since the properties of solid particles are of great importance, a single source of erodent particles was used throughout the experiments. Also, fresh particles were used in each test to avoid any degradation of impacting particles during erosion tests. In these series of tests, the particles concentration was held at 1 wt% and the impact velocity of slurry stream was 15 m/s.

The difference between the apparatus used in the current study- slurry whirling arm rig - and the other apparatus used in this field is the absence of dependence on time in the present apparatus regarding the comparison among the different impact angles. As shown in Figure 2, the amount of particles which impact the surface of specimen differs from angle to another.

It is important to emphasize that, comparing the effect of different impact angles on the erosion rate at the same test-time will give misleading results. This is due to the fact that, at the same test-time the amounts of particles which impact the surface of the specimen differ at different impact angles. Therefore, the comparison will be performed through subjecting the specimens at all the impact angles to the same amount of particles. In this case, the test time will be different from angle to another. Therefore the erosion rate is defined as that corresponding with the mass loss from a specimen subjected to impact by an assumed fixed mass of slurry particles. The amount of particles which impact the surface of specimen as a function of the impact angle is derived from the geometry of the impacting process, as shown in Figure 2 [13].

So, the mass of particles striking each specimen per one revolution is given by;

$$m_p = \left[l \sin(\theta_o) A_n + \frac{l \cos(\theta_o) Q}{\pi DN} \right] C_w \rho_w \dots\dots\dots (1)$$

Where,

θ_o : the angle between the surface plane of the specimen and the horizontal plane [13].

- l : is the length of wear specimen surface in m,
- A_n : is the area of orifice in m^2 ,
- C_w : is the weight fraction of solid particles in the water,
- ρ_w : is the water density in kg / m^3 ,
- D : is the rotational diameter of the wear specimen m,
- Q : is the volume flow rate of slurry in $m^3/min.$, and
- N : is the rotational speed of the wear specimen in rpm.

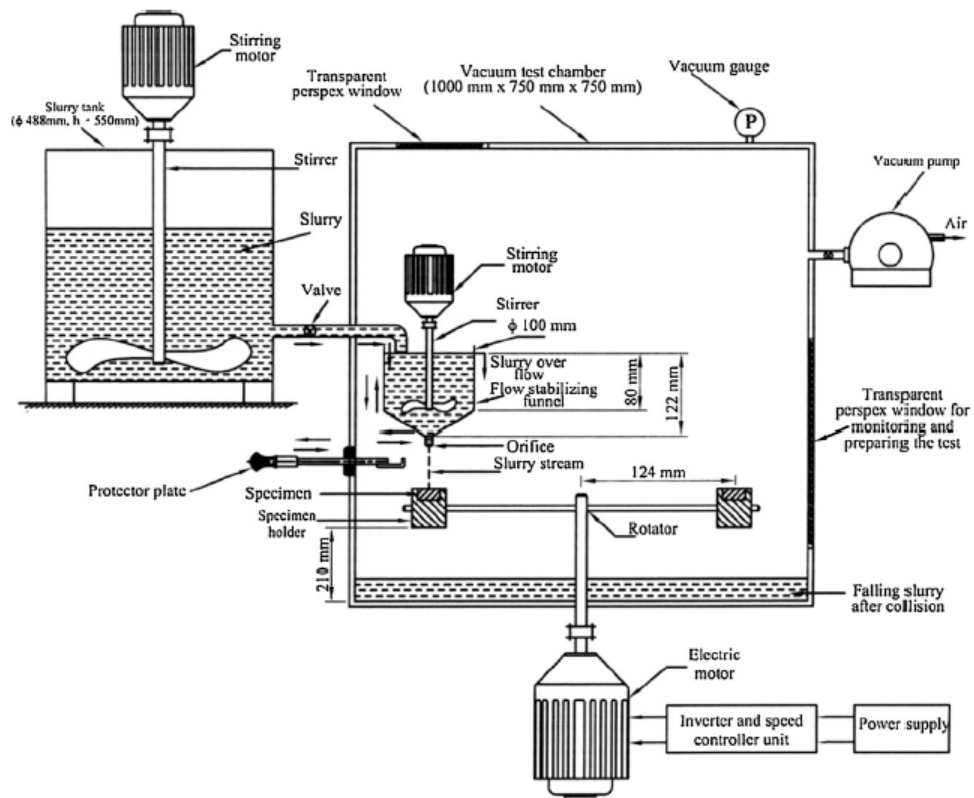


Figure 1 Schematic diagram of the designed slurry erosion whirling-arm rig

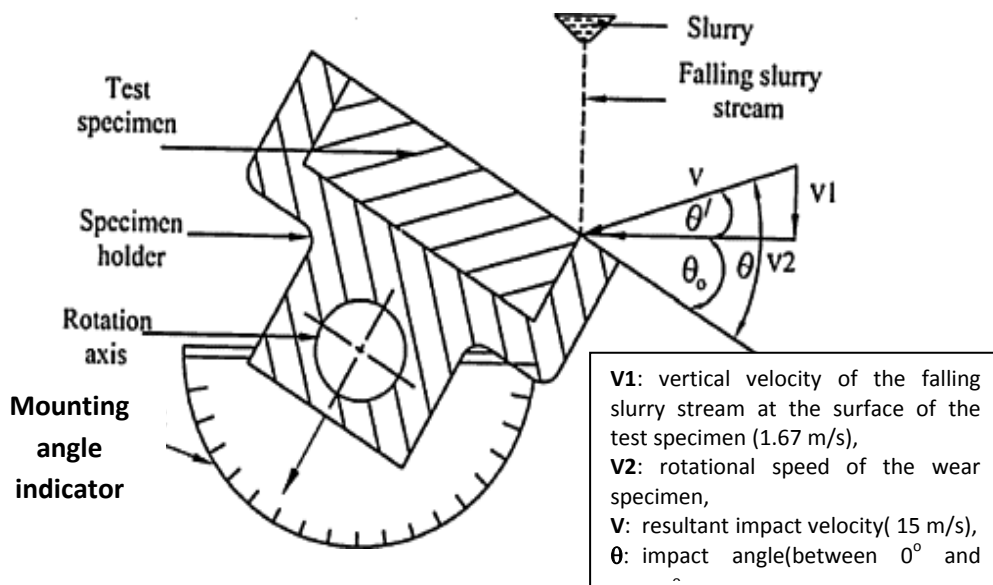


Figure 2 Schematic diagram of impact velocity and impact angle

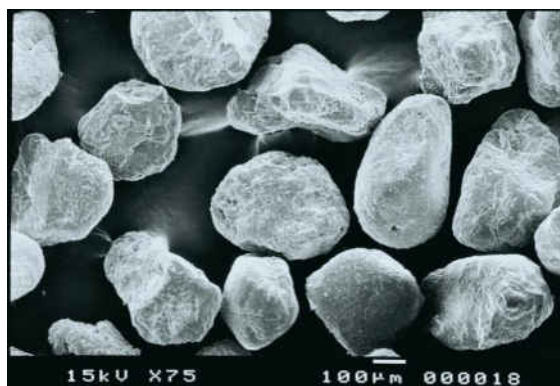


Figure 3 Scanning electron microphotograph of silica sand (size range, 250-355 μm)

Two types of erosion tests were carried out, namely: long and short tests. The long tests mean that the specimens were exposed for large quantities of solid particles and in the short tests the specimens were exposed for smaller amount of solid particles. Long tests were carried out to study the effect of impact angles on the erosion rate. Short tests were carried out to study the mechanism of metal removal of carburized steel specimens due to slurry erosion. At each impact angle a series of successive tests were carried out. In each test a little mass of erodent of about 1.3 g was allowed to impact the specimen. After each test, isolated individual impact events were examined. In order to clarify the metal removal mechanism the subsequent impact events at

successive stages were also studied. The features of eroded surfaces were examined by scanning electron microscope (SEM) JEOL JSME 5400

3. Results and discussion

3.1 Microstructure

SEM micro photo graphs of the microstructure of carburized steel specimens at 6 and 12 h are shown in Figure 4. From these photos the treated layer can be easily distinguished from the core material. As can be seen in the Figure 4, the carburized case depths are approximately 0.65 and 0.95 mm for 6 and 12 h treated material, respectively. It can also be observed that microstructure near the surface is martensitic with small amount of retained austenite for treatment time of 6 h (Figure4 (a)). For the treated specimen for 12 h, microstructure near the surface is almost completely martensitic due to the high carbon content and again small amount of retained austenite can be seen as well, Figure 4 (b).

The core microstructures of carburized steels are determined by the low carbon content and base hardenability of the carburized steel. Depending on quenching rate the low-carbon core may transform to ferrite with small of amount of pearlite or the core may transform to martensite. Due to the direct quenching to the room temperature, the core was transformed to martensite, in present work. Low-carbon martensite has higher strength and fracture resistance or toughness than do ferrite-pearlite microstructures. This increased strength is necessary to prevent subsurface crack initiation, sometimes referred to as case crushing. Tempering is the final heat treatment step, which increases toughness slightly and relieves some residual stresses, but case hardness is largely preserved. The major change of the microstructure is the precipitation of transition carbide from the martensite supersaturated with carbon by quenching. This carbide precipitates in rows of very fine particles, about 2 nm in size, within the martensite plates. These microstructural changes are too fine to be resolved in the light microscope, but are reflected by an increased tendency of the martensite plates to appear black [16].

Figure 5 is a SEM micrograph showing the typical martensite – austenite microstructure formed close to the surface of carburized steels. The high-carbon martensite (appears dark in the photo) is formed by diffusion-less and shear transformation of the austenite. The white areas of Figure 5 are regions of austenite that have not transformed. This austenite is referred to as retained austenite and is present because of the high stability of high carbon austenite. Retained austenite plays a significant role in the fatigue of carburized steels [16].

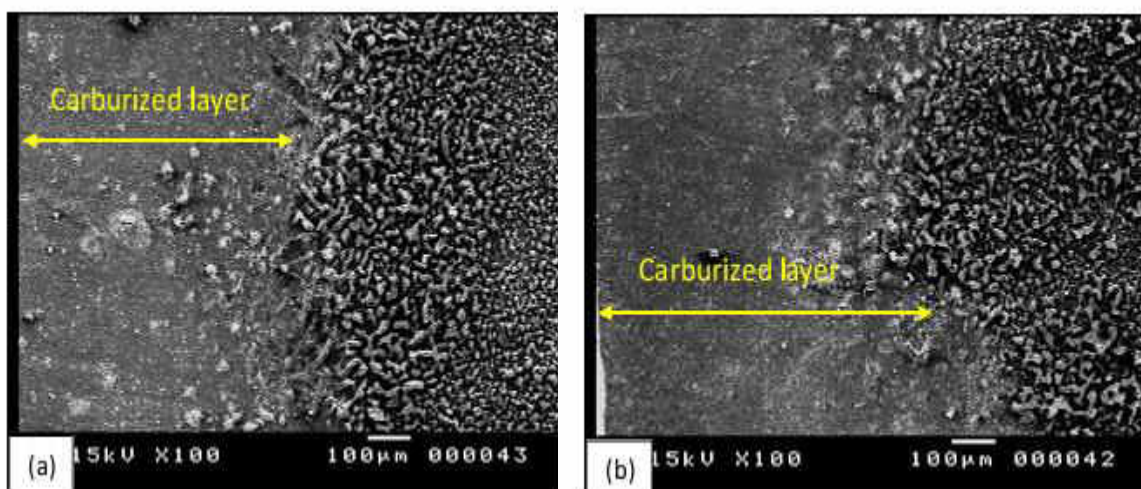


Figure 4 SEM micro photo graphs showing microstructures of (a) Carburized case depth for 6 h and (b) carburized case depth for 12 h

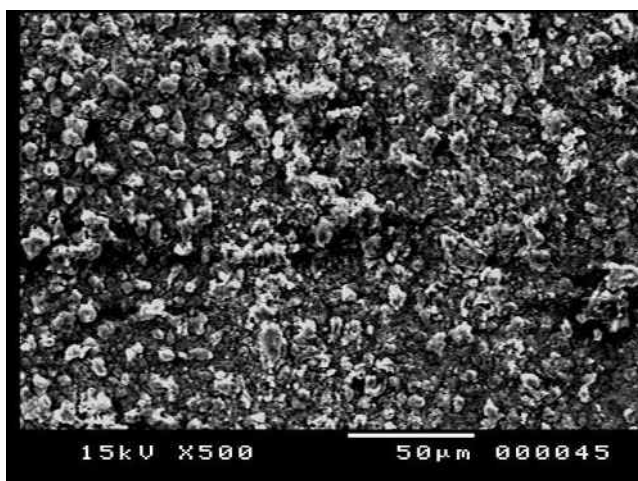


Figure 5 SEM micrograph showing martensite-austenite microstructure in case of carburized steel AISI 5117

3.2 Hardness profile

Figure 6 shows micro-hardness profiles obtained from cross sections of treated and untreated samples as function of depth. The hardness at or near the surface attains to more than approximately 883 HV and 950 HV in the 6 and 12 h treated materials, respectively. The hardness of the untreated specimen is 200 HV and is constant with depth. The hardness of treated materials decreases gradually with the depth and reaches a constant value at the cores. The hardness at the cores is 473 HV and 430 HV in treated materials for 6 and 12 h, respectively.

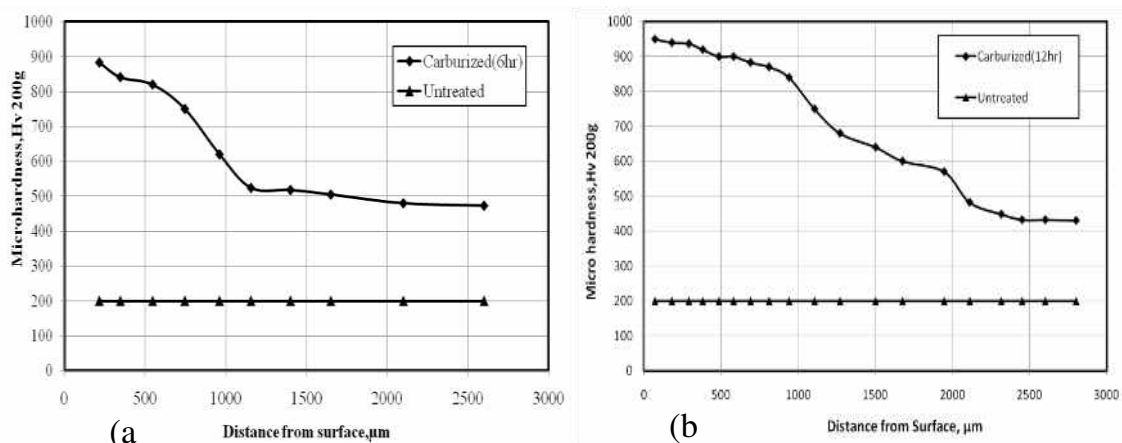


Figure 6 Hardness distribution of treated and untreated material:
(a) treated for 6 h and (b) treated for 12 h

3.3 Slurry Erosion behaviour

Figures 7 and 8 (a, and b) show the relationship between the mass loss and impact angle for different masses of erodent for the untreated and the carburized specimens. All the erosive wear curves for the untreated and the carburized specimens show similar characteristic features. It is clear from the results that the increased surface hardness has resulted in lower mass losses. The highest mass losses are obtained in the untreated specimen. The mass loss for all specimens show a similar variation tendency, in which the erosion rate increases and then decreases with increasing impact angle from 30° to 90° and reaches a maximum around 45°. It shows a typical ductile erosion behavior [17-20]. For ductile materials, impact at low impact angles will increase material removal by microcutting because of the oblique shear force [12,21], thus increasing the mass loss. At high impact angles, the resolved normal stress will produce the accumulated damage mainly from fatigue [22], microforging, and extrusion processes [23]. These processes can only produce slighter erosion damage than that caused by cutting removal at low impact angles. Hence, there appears a maximum mass loss at around 45°. These features will be highlighted in the next section. As shown in Figs. 7 and 8(a, and b), the carburized specimens show less erosion rates. Furthermore, the erosion rate of the carburized specimens decreases with increasing carburizing holding time: i.e., the mass loss decreases with increase of the case depth and surface hardness. This improvement is effective even at high impact angles because increasing surface hardness after carburizing is not accompanied by loss in ductility of the material substrate [24].

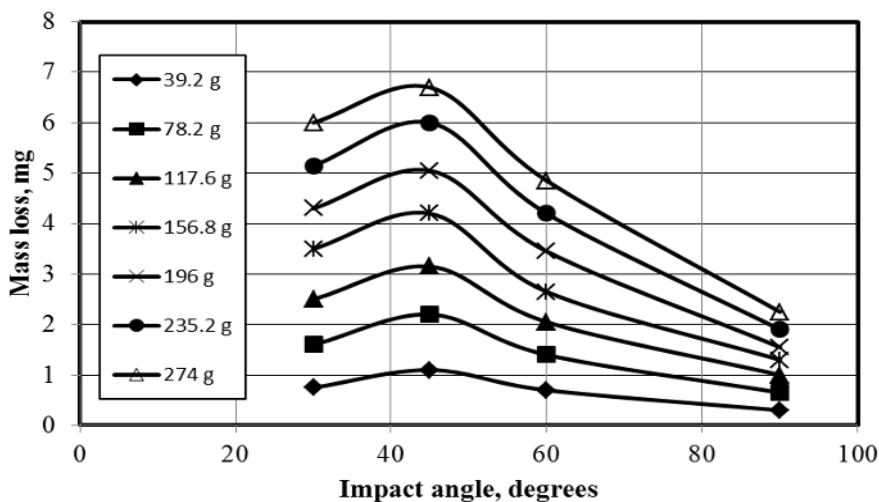


Figure7 Relationship between the mass loss of untreated material and impact angles for different masses of erodent

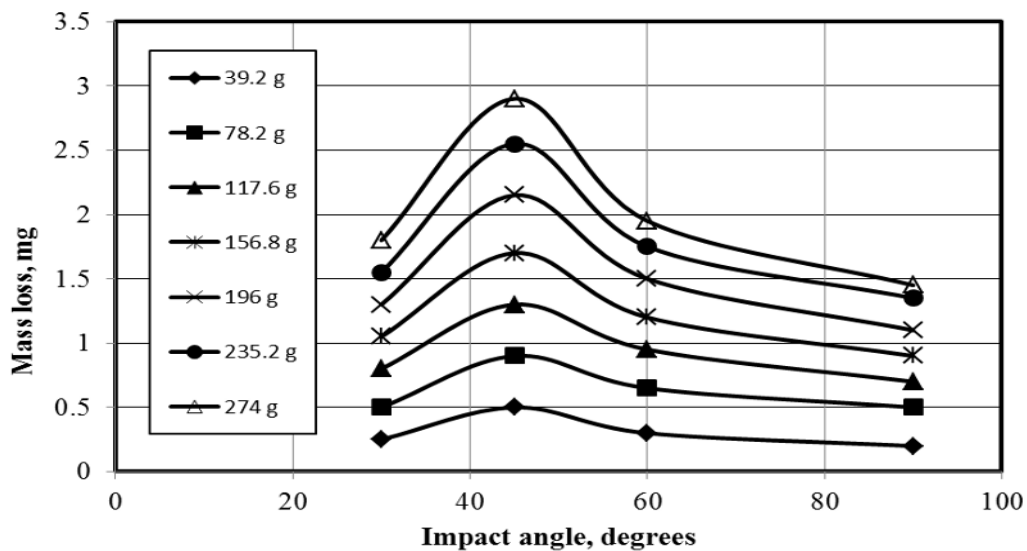


Figure 8a Relationship between the mass loss of carburized specimens at 950°C for 6 h and impact angle for different masses of erodent.

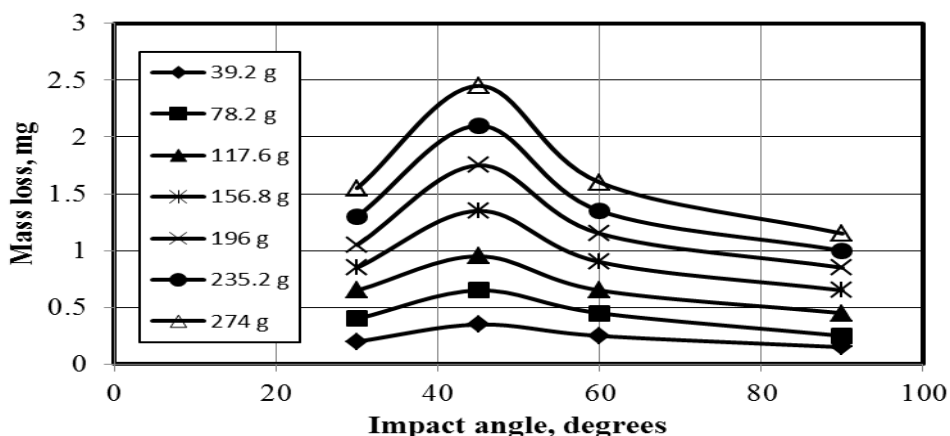


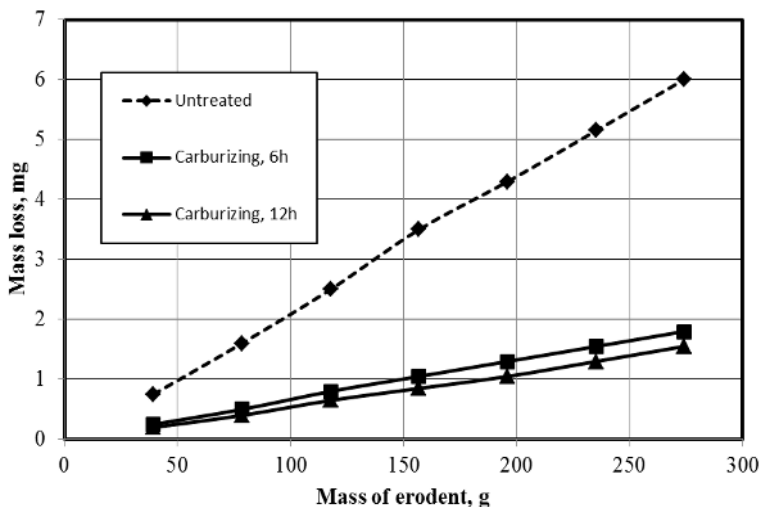
Figure 8b Relationship between the mass loss of carburized specimens at 950°C for 12 h and impact angle for different masses of erodent

To throw more light on the effect of carburizing on the enhancement of erosion resistance, the mass losses of treated and untreated specimens versus the mass of erodent at each impact angle are presented in Figure 9(a – d). From these Figures, it is observed that the mass loss as function of mass of erodent for untreated specimen is always more than treated one at all impact angles. This difference in the mass loss between untreated and treated material generally decreases with the increase of the impact angle. For mass of erodent 274 g, the difference in the mass loss between the carburized for 6 h and untreated materials is 4.2, 3.8, 2.9, and 0.8 mg at an impact angle of 30°, 45°, 60° and 90°, respectively. Therefore, the erosion resistance of AISI 5117 steel increases by 70, 57, 60 and 36 % at an impact angle of 30°, 45°, 60°, and 90°, respectively as result of carburizing for 6 h. As result of carburizing for 12 h the erosion resistance of AISI 5117 steel increases by 74, 63, 67, and 49% at an impact angle of 30°, 45°, 60°, and 90°, respectively. Based upon these results, it can be concluded that the carburizing process enhances the erosion resistance of AISI 5117 steel. The enhancement of carburized material is maximum at small impact angles (30°) and decreases almost continuously with the increase of the angle down to a minimum at 90° at the test conditions used in the experiments. The reason behind the high erosion resistance of the carburized specimens compared to the untreated ones can be attributed by the increase in hardness and the change of the microstructure of the former, as will be illustrated in the next section. The higher microhardness can effectively block the interaction and propagation of cracks in the carburizing layer. The fine carbides participated in rows, due to the tempering of carburizing specimens, is tough enough to survive the particle impact; hence, they show minimum slurry erosion compared with the untreated specimens.

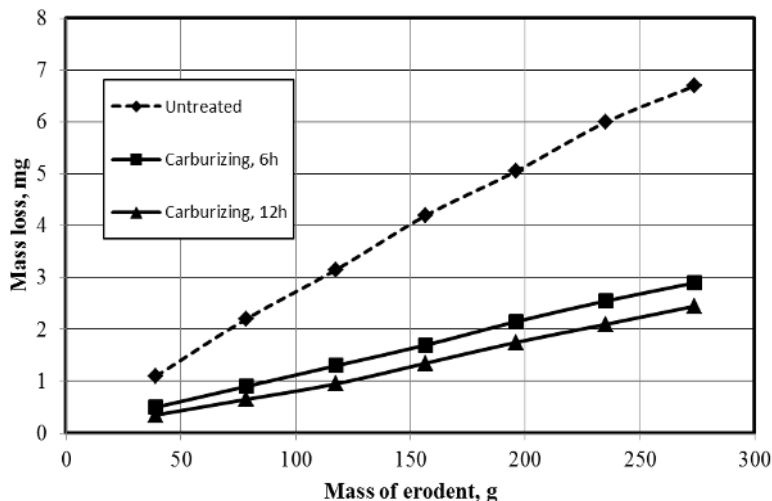
Therefore, in hydraulic equipment made of low carbon alloy steel it is recommended to carry out carburizing to surfaces subjected to slurry erosion especially

when the angle of impact is low or intermediate. At normal impact angle the economic effect must be studied.

It can be observed from Figure 9(a-d) that the mass losses are found to increase linearly with increasing erodent mass for treated and untreated specimens. This illustrates that the erosion mechanism does not change noticeably, implying a steady erosion damage during the impact process, regardless of the variation in the impact angle.

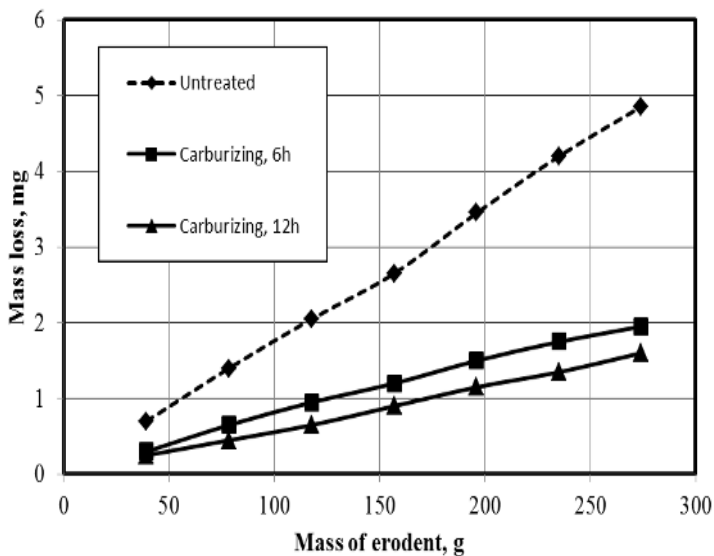


(a)

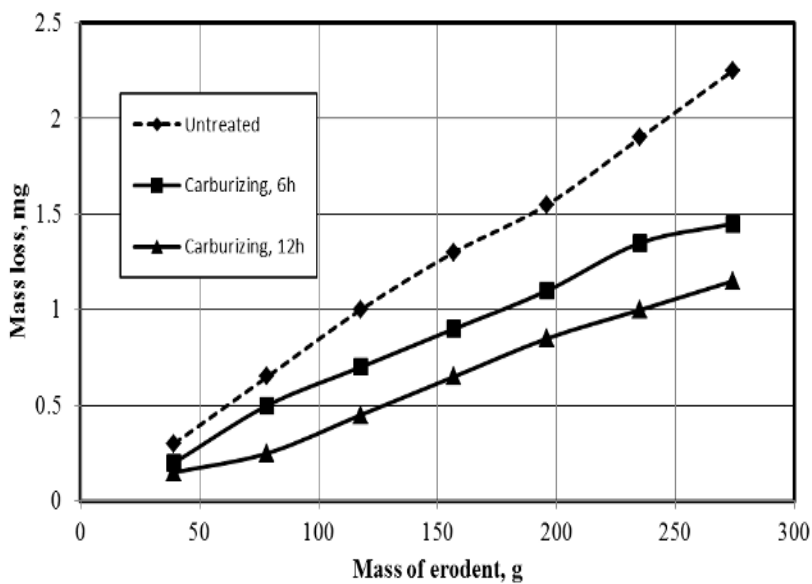


(b)

Figure9 Mass loss of treated and untreated specimens versus mass of erodent at different impact angles: (a) 30°, (b) 45°, (c) 60° and (d) 90°.



(c)



(d)

Figure 9 Continued.

3.4 Aspects of eroded surfaces

The morphologies of the eroded surfaces of the untreated and treated specimens at different impact angles and mass of erodent of 3.9 g are shown in Figure10 (a and b) Due to the low hardness, the surface of the untreated specimens are severely deformed during the erosion test for all impact angles, but in the same time the degree of erosion differs with impact angle as shown in Figure10(a). It can be seen from Figure 10 (a and b) that the erosion tracks developed on the untreated specimens are the wider and deeper than that formed on the carburized specimens. Furthermore, the erosion tracks of the carburized specimens are shallower and more superficial Figure10(b). The wear test results, shown from this figure and that presented in Figs. 7-9, revealed that on carburization, wear resistance of carbon steel improved greatly over that in the untreated state. These changes in wear properties of steel are being primarily controlled by alteration in its carbon content, hardness and microstructure [25]. For treated and untreated specimens, the erosion tracks are formed by ploughing and microcutting for acute angles and by material extrusion for normal impact angle.

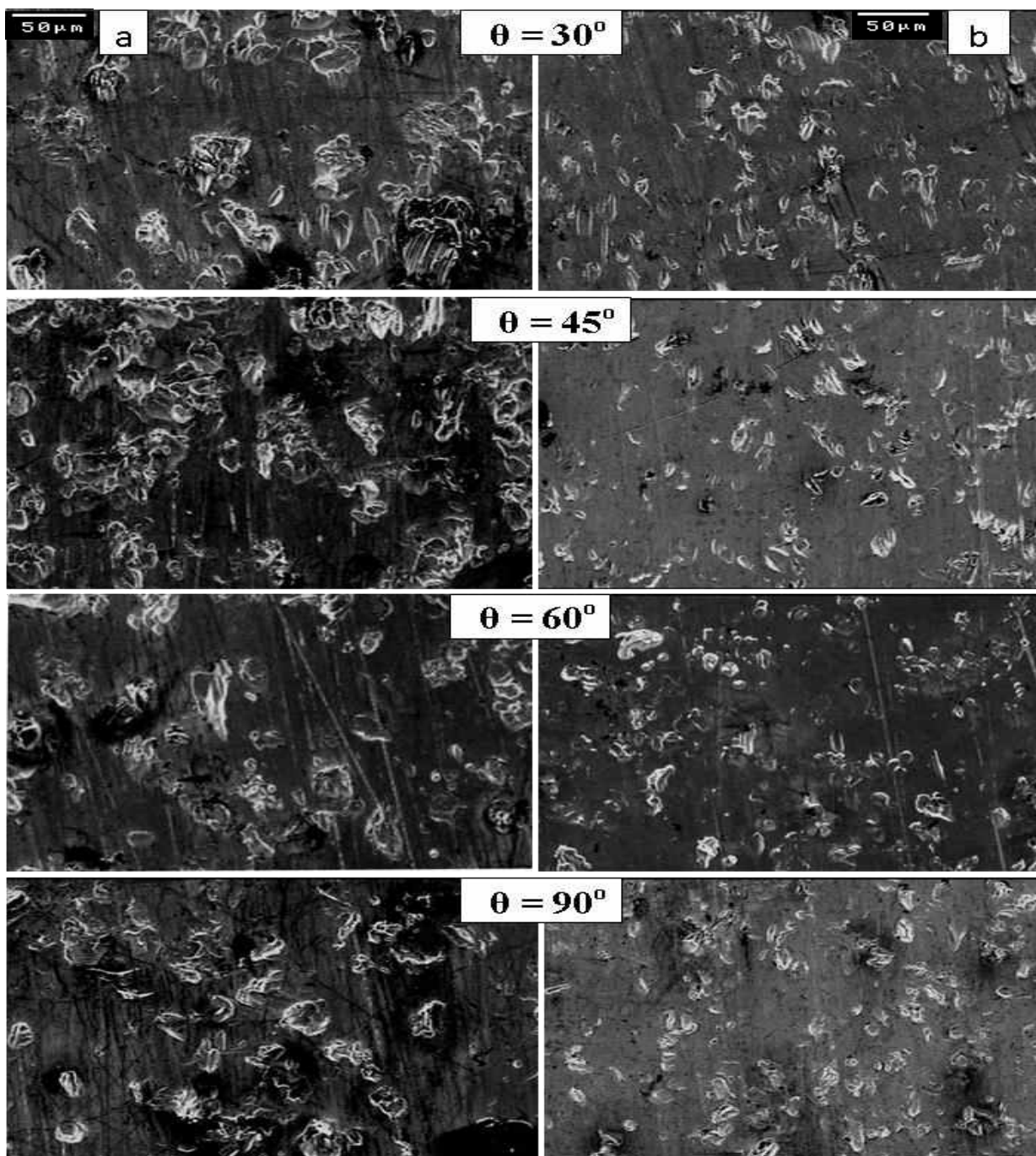


Figure 10 SEM features of eroded surfaces of treated (b) and untreated (a) steel at different impact angles

3.5 Tracking the removal process

To give practical and visible evidence of how the damage to be developed with subsequent impacts, systematic microphotographs for four successive stages were taken. The amount of erodent which impacts the specimen was 1.3 g for each stage at impact angles of 30°, 45°, 60° and 90°. The results are presented in Figs. 11 and 12. The white areas in these microphotographs represent the impact sites. The inclined vertical lines shown in these photos are the traces of polishing lines. These photos illustrate that the shape of impact sites depend upon the angle of impact. This accentuates the previous findings about the change of erosion mechanism with impact angle. Some of the impact sites are formed with directionality. This directionality is in the direction of slurry stream at small impact angles $\theta = 30^\circ$ and 45° ; but for angles larger than 45° this directionality shows some deviation from the slurry stream direction. This can be referred to impacting particle dynamics [12, 13]. At any given stage and angle in Figure 11, it is easy to see that the impact sites have different sizes. Some of these sites appear to be shallow and the others are relatively deep. This can be explained in the light of the effect of particle size range, particle trajectory and material structure. The particles have the size range of 250-355 μm , so the kinetic energy will be differed by about 27% from small to large size range. The particle-wall collisions, which influence particle motion [26] will lead to the change in the actual impact angle and impact velocity from the nominal values. The examination of slurry erosion behavior of subsequent stages shown in Figs. 11 and 12 reveals that the particle impact processes include the following events; forming new impact sites, impacting former sites and impacting the surface but without noticeable effect. The new impact sites that are formed in the subsequent stages, after stage no. 1, are encircled as shown in Figs. 11 and 12. The number of impact sites versus the mass of erodent is not carried for carburized material, but it is measured for untreated material [27]. It was found that the number of impact sites is more in low impact angle compared with high impact angle. This may be explained in the light of particle rebound effect. The coefficient of restitution decreases with the increase of impact angle [26]. When new particles impact former impact sites, the chips and the extruded materials formed at low and high impact angle, respectively, in the impact sites will be detached. Under subsequent impacts for these sites, it was observed that in some of the impact sites craters were formed and the others disappeared. For particles that have a small kinetic energy and are not able to create visual effects on the surface, this does not mean that these particles have no role in the process of erosion, but they lead to the surface hardening.

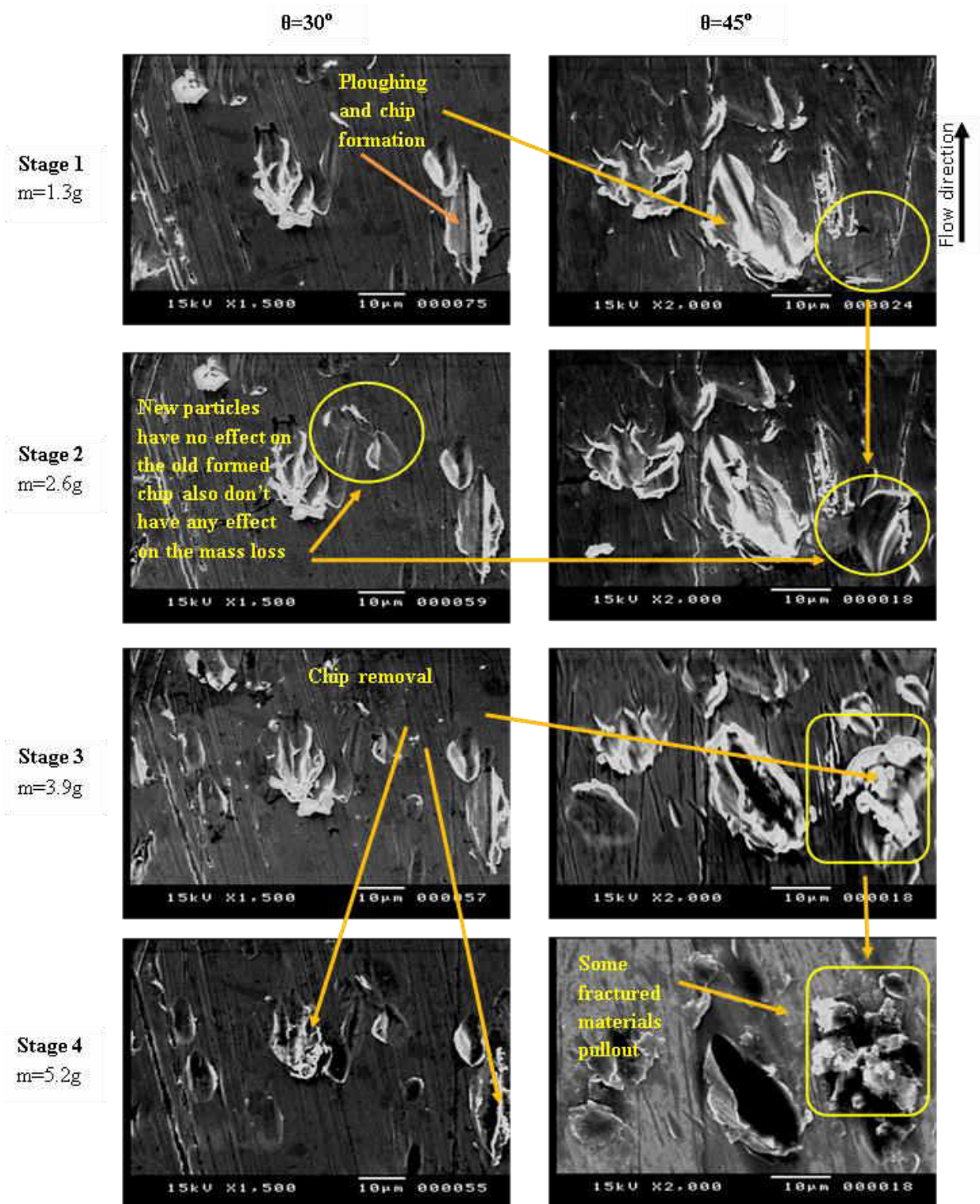
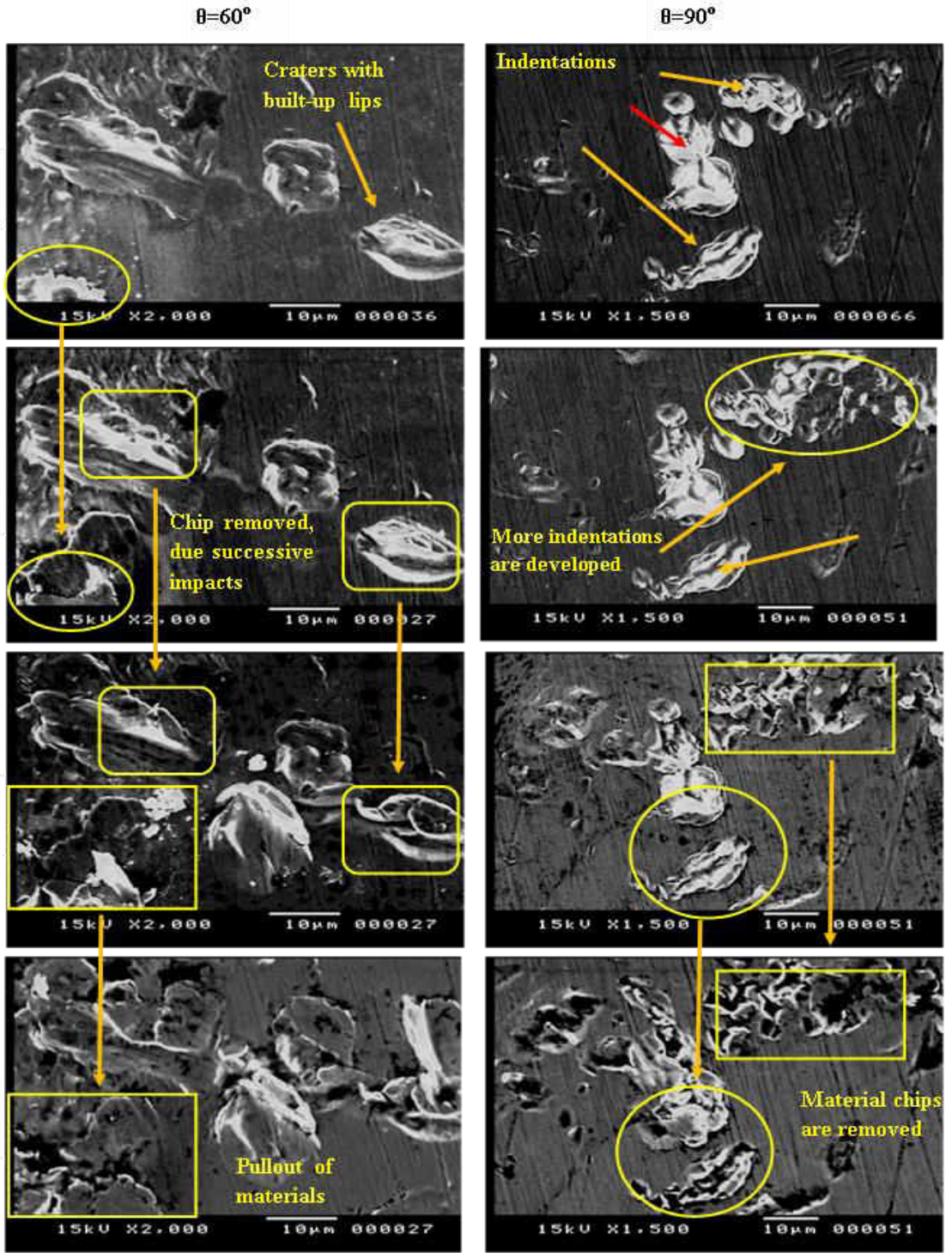


Figure 11 SEM microphotographs of carburized steel AISI 5117 impacted at low



impact angles, $\theta=30^\circ$ and 45° .

Figure 12 SEM microphotographs of carburized steel AISI 5117 impacted at high impact angles, $\theta=60^\circ$ and 90°

4. Conclusions

The slurry erosion behavior and operating erosion mechanisms of carburized steel AISI 5117 were studied using a slurry whirling arm erosion test rig. The following conclusions can be drawn out:

1. The carburized specimens show a much better slurry erosion resistance than the untreated specimen, even at higher impingement angles. In addition, the mass loss of the carburized specimens is decreased with increasing the carburizing holding time, which is attributed to the increase of the case depth and surface hardness.
2. The treated and untreated materials show a ductile behavior and the maximum mass loss appears at an impingement angle of 45°.
3. Plough grooves and cutting lips appear in the eroded surfaces at acute impact angle, while material extrusions occur at normal impact. The erosion traces on the untreated specimens are wider and deeper. However the erosion traces of carburized specimens are shallower and more superficial. This feature leads to the decrease of erosion rate.

5. References

- [1] Q. Fang, Microripple Formation and Removal Mechanism of Ceramic Materials by Solid-Liquid Slurry Erosion, *Wear* 223 (1998) 93-101.
- [2] S. Lathabai, and D. C. Pender, Microstructure influence in slurry erosion of ceramics *Wear* 189 (1995) 122-135.
- [3] Y. Li, G.T. Burstein, and I. M. Hutchings, The Influence of Corrosion on the Erosion of Aluminum by Aqueous Silica Slurries, *Wear* 186-187 (1995) 515-522.
- [4] Y. Iwai, and K. Nambu, Slurry Wear Properties of Pump Lining Materials, *Wear* 210 (1997) 211-219.
- [5] W. Tsai, J. A. C. Humphrey, I. Cornet, and A. V. Levy, Experimental Measurement of Accelerated Erosion in a Slurry Pot Tester, *Wear* 68 (1981) 289-303.
- [6] B. Stanisa, and V. Ivusic, Erosion Behaviour and Mechanisms for Steam Turbine Rotor Blades, *Wear* 186-187 (1995) 395-400.
- [7] B. Selcuk, R. Ipek, and M. B. Karamis, A Study on Friction and Wear Behavior of Carborized, Carbonitridid and Borided AISI 1020 and 5115 Steels, *J. Mater. Process. Technol.* 141 (2003) 189-196.
- [8] S.K. Patel, and M. Kumar, Erosive Wear Characteristics of Carburized Mild Steel in Soil – Water Slurry, Proc. of the 4th International Conference on Advances in Mechanical Engineering, S.V. National Institute of Technology, Surat – 395 007, Gujarat, India. September 23-25 (2010) 1-5.
- [9] J. Gupta, Mechanical and Wear Properties of Carburized Mild steel Samples, Master thesis, Dep. of Mech. Eng. National Inst. OF Techn., Rourkela, India, (2009)
- [10] R.C. Shivamurthy, M. Kamaraj, R. Nagarajan, S.M. Shariff, and G. Padmanabham, Slurry Erosion Characteristics and Erosive Wear Mechanisms of Co-Based and Ni-Based Coatings Formed by Laser Surface Alloying, *Metallurgical and Materials Transactions A.* 41 (2009) 470-486.
- [11] Bohler, Special Steel Manual, A-8605 Kapfenberg, Germany, (2000) 90–98.

- [12] M. A. Al-bukhaiti, S. M. Ahmed, F. M. F. Badran, K. M. Emara, Effect of Impingement Angle on Slurry Erosion Behaviour and Mechanisms of 1017 Steel and High-Chromium White Cast Iron, *Wear* 262 (2007) 1187-1198.
- [13] A. Abouel-Kasem, Y. M. Abd-Elrhman, S. M. Ahmed, and K. M. Emara, Design and Performance of Slurry Erosion Tester, *ASME J.Tribol.* 132(2) (2010) 021601.
- [14] A. Abouel-Kasem, M. A. Al-bukhaiti, S. M. Ahmed and K. M. Emara, Fractal Characterization of Slurry Eroded Surfaces at Different Impact Angles, *ASME J.Tribol.* 131 (2009) 1-9.
- [15] A. Abouel-Kasem, Particle Size Effects on Slurry Erosion of 5117 Steels, *ASME J.Tribol.* 133 (2011) 014502-1
- [16] G. Krauss, Microstructure and Properties of Carburized Steels, ASM International, Heat treatment Hand book, Vol. 4, (1991) 832-836.
- [17] H. M. Clark, Test Method and Applications for Slurry Erosion - a Review, *Tribology.* ASTM, STP 1199 (1993) 113-132.
- [18] J. B. Zu, I. M. Hutchings, and G. T. Burstein, Design of a Slurry Erosion Test Rig, *Wear* 140 (1990) 331-344.
- [19] G. Burstein, Effect of Impact Angle on the Slurry Erosion–Corrosion of 304L Stainless Steel, *Wear* 240 (2000) 80-94.
- [20] H. C. Lin, S. K. Wu, and C. H. Yeh, A comparison of Slurry Erosion Characteristics of TiNi Shape Memory Alloys and SUS 304 Stainless Steel, *Wear* 249 (2001) 557-565.
- [21] I. Finnie, D.H. McFadden, On the Velocity Dependence of the Erosion of Ductile Metals by Solid Particles at Low Angles of Incidence, *Wear* 48 (1978) 181–190.
- [22] I.M. Hutchings, A Model for the Erosion of Metals by Spherical Particles at Normal Incidence, *Wear* 70 (1981) 269–281. A Adler, O.N.
- [23] R. Bellman Jr., A. Levy, Erosion mechanism in ductile metals, *Wear* 70 (1981)1–27.
- [24] D.C. Wen, Erosion and Wear Behavior of Nitrocarbured DC53 Tool Steel, *Wear* 268 (2010) 629-636.
- [25] H. M. Clark, and K. K. Wong, Impact angle, particle energy and mass loss in erosion by dilute slurries", *Wear* 186–187 (1995) 454–464.
- [26] S.K. Patel and M. Kumar, Erosive Wear Characteristics of Carburized Mild Steel in Solid-Water Slurry, Proc. 4th Int. Conf. Advances in Mechanical Engineering, S.V. Nat. Inst. Of Tech., Surat, Gujarat, India.(2010)
- [27] Y. M. Abd-Elrhman, A. Abouel-Kasem, S. M. Ahmed, and K. M. Emara, , Stepwise Erosion as a Method for Investigating the Wear Mechanisms at Different Impact Angles in Slurry Erosion, *J. Eng. Sci., Assiut University-Egypt*, 40(4) (2012) 1055-1074.

تأثير زاوية التصادم على سلوك وآليات التآكل بالنحر لصلب الفولاذ (AISI 5117) المعالج حرارياً بالكربون

يقدم هذا البحث دراسة عن التآكل بالنحر لصلب الفولاذ (AISI 5117) المعالج حرارياً بالكربون (عملية الكرينة) بإستخدام جهاز التآكل ذي الذراع الدوار. تركز الدراسة بصفة أساسية على دراسة خصائص مقاومة التآكل بالنحر لصلب الفولاذ (AISI 5117) المكربن عند زوايا التصادم المختلفة و بإستخدام مجهر الماسح الالكتروني لفحص العينات المتآكلة. كما ان صور الماسح الالكتروني للعينات المتآكلة عند المراحل المختلفة تم عرضها لزيادة فهم آليات التآكل عند زوايا التصادم المختلفة. تم تنفيذ الاختبارات بإستخدام حبيبات صلبة بتركيز 1%، وسرعة تصادم للسائل المتدفق المحمل بالحبيبات الصلبة 15 م/ث. سيلكا الرمل المستخدمة لصدمة العينات يتراوح حجمها من 250-355 ميكرومتر. بينت النتائج ان عملية الكرينة للحديد تزيد من الصلادة والمقاومة للتآكل بالنحر مقارنة بالمواد الغير معالجة عند كل زوايا التصادم. مقاومة التآكل بالنحر كنتيجة لعملية الكرينة لصلب الفولاذ (AISI 5117) زادت بنسبة 70, 57, 60, 36 % عند زوايا تصادم 30, 45, 60, 90 درجة، بالترتيب. أى ان أعلى كفاءة لعملية الكرينة عند زوايا التصادم المنخفضة. العينات المعالجة بالكربون والغير معالجة تتصرف كمواد مطيئة، أى أن اكبر معدل تآكل بالنحر يظهر عند زاوية تصادم 45°. الاخاديد المحروثة والشفاه المقطوعة تظهر عند زوايا التصادم الحادة، ولكن يحدث إنبثاق للمعدن عند زوايا التصادم العمودية. آثار التآكل بالنحر أوسع وأعمق للمواد غير المعالجة مقارنة بالآثار الضيقة والسطحية للعينات المكربنة.

كلمات البحث:

التآكل بالنحر، عملية الكرينة، زاوية التصادم، صلب الفولاذ (AISI 5117)، مقاومة التآكل، آليات التآكل بالنحر.